Physics AUC, vol. 19, 22-34 (2009)

PHYSICS AUC

Energy transfers in magnetohydrodynamic turbulence in presence of an ambient imposed magnetic field

B. Teacă[1,3]*, M. K. Verma [2] †& D. Carati [3] ‡,

[1]Faculty of Physics, University of Craiova, A.I. Cuza 13, 200585 Craiova, România

[2]Department of Physics, Indian Institute of Technology, 208016 Kanpur, India

[3]Statistical and Plasma Physics, Université Libre de Bruxelles, Campus Plaine, CP 231, B-1050 Brussels, Belgium

Abstract

The purpose of this study is to explore the energy exchange mechanisms in magnetohydrodynamic (MHD) turbulence. A spectral analysis of isotropic and anisotropic MHD turbulence is performed using direct numerical simulations. The anisotropy is generated due to the presence of the ambient magnetic field and the turbulence level is maintained by a mechanical force. In the statistically stationary regime, the energy spectra and the energy transfer functions are studied for different values of the ambient magnetic field. In the direction parallel to this magnetic field, we observe suppression of the energy transfer when compared to the isotropic case. Also the energy tends to accumulate around the direction perpendicular to the constant magnetic field. These effects are stronger with the increase of the constant magnetic field value. Since the use of shell-to-shell transfer functions is inadequate for describing anisotropic effects, a ring decomposition of the spectral space is used.

1 Introduction

Usually, in a fluid or a plasma, the global energy sources (mechanical forcing, heating, etc.) and the global energy losses (dissipation mechanisms, plasma-wall interactions, etc.) are fairly easily identified. However, determining how the energy is stored and distributed in the system is a much more difficult task. The purpose of this study is to explore the energy exchange mechanisms in the fluid limit of a conductive medium described by the magnetohydrodynamic (MHD) formalism. In order to simplify the picture as much as possible, we will focus on incompressible MHD, for which the total energy (E^t) has two components: the kinetic (E^u) and the magnetic (E^b) energies. For compressible turbulence, the internal energy has also to be taken into account. The characterization of energy exchanges can be helpful for the validation of theoretical approaches and the development of simplified models.

*Electronic mail: bteaca@ulb.ac.be

†Electronic mail: mkv@iitk.ac.in

‡Electronic mail: dcarati@ulb.ac.be

Talk given at International Workshop "Anomalous Transport in Fusion Plasmas", October 6-8, 2008, Craiova, Romania

In order to describe the mechanisms of energy transfer, the usual strategy is to decompose the domain in which the velocity and the magnetic field are defined into sub-domains. Numerical simulations can then be used to measure the energy exchanges between the sub-domains. The definition of the sub-domains will be adapted to the nature of the problem. Two main strategies can be adopted. A decomposition of the physical domain or a splitting of the dynamical variables based on the characteristic length scales, such as the Fourier decomposition. The physical space decomposition is more useful for deriving models for complex geometries and boundary problems while a Fourier decomposition provides a better insight into the physical phenomena of energy transfer. A wavelet analysis could also be considered and would provide an hybrid approach in which the decomposition would couple the physical space and the characteristic length scales. In the following study, we will focus on a decomposition of the Fourier space into sub-domains. Because the Fourier modes are only coupled through the nonlinear terms in the MHD equations, energy exchanges will be of particular importance when these nonlinear terms are dominant, especially for turbulent systems.

The energy transfers between modes in turbulence are completely characterized by triad interactions [1]. Since the majority of modes have similar properties as their wave-number neighbors and bring similar contribution to the energy exchange between scales, the analysis of energy transfers is usually simplified by partitioning the spectral space into sub-domains and look at the averaged energy transfers between these sub-domains [2]. The partitioning of the spectral domain is arbitrary but several convenient geometrical structures are preferred. The spectral spherical symmetry present in the case of isotropic turbulence naturally suggests a decomposition of the spectral domain into wave-number shells. For this case the energy transfer is described in terms of shell-to-shell transfer functions and spherical energy fluxes that have been studied in details [3, 4, 5]. In the presence of a mean magnetic field, the flow develops a preferred direction and exhibits anisotropy. The degree of anisotropy depends on the strength of the mean magnetic field. The angular dependence with respect to the preferred direction then becomes as relevant as the wave vector amplitude in the spectral space partition, and a simple shell decomposition may not be appropriate any more. Coaxial cylindrical domains aligned with the preferred direction and planar domains transverse to each direction have both been used in the past to partition the spectral space [6]. In this work, we also use another partition that is based on a ring decomposition of shells. Similar to the scheme proposed by Alexakis et al. [6], the present approach provides many details on the energy transfers in an anisotropic system. This information should help the understanding of the anisotropic turbulence dynamics that in turn will help in the development of LES models for MHD turbulence. Moreover, the present approach allows to recover easily the isotropic transfer functions which have been extensively studied in literature.

2 Theoretical framework

The MHD equations for a fluid read in the incompressible limit as

$$\frac{\partial u_i}{\partial t} = -u_j \nabla_j u_i + B_j \nabla_j B_i + \nu \nabla^2 u_i + f_i - \nabla_i p \,, \tag{1}$$

$$\frac{\partial B_i}{\partial t} = -u_j \nabla_j B_i + B_j \nabla_j u_i + \eta \nabla^2 B_i \,, \tag{2}$$

where $u_i = u_i(\mathbf{x},t)$ is the fluid velocity field, $B_i = B_i(\mathbf{x},t)$ is the magnetic field expressed in Alfvèn units and $p = p(\mathbf{x},t)$ is the total, hydrodynamic and magnetic, pressure field

divided by the constant mass density. The magnetic field B_i is the sum of a constant part B_i^0 and a turbulent part b_i induced by the flow. The fluid viscosity ν and the magnetic diffusivity η are taken to be equal, so that the magnetic Prandtl number (Pr = ν/η) is unity. The divergence free force $f_i = f_i(\mathbf{x},t)$ used in the present work is chosen to be isotropic so that it does not introduce any preferred direction. The equations (1)-(2) are supplemented by the incompressibility condition for the fluid ($\nabla_j u_j = 0$) and the divergence-free condition for the magnetic field ($\nabla_j b_j = 0$). By convention, summation over repeated indices is assumed. Because of the incompressibility condition, the pressure p can be formally eliminated by solving the Poisson equation:

$$\nabla^2 p = -\nabla_i u_j \nabla_j u_i + \nabla_i b_j \nabla_j b_i. \tag{3}$$

In order to describe the dynamics of energy transfers in MHD turbulence, the equations (1-2) are solved in a periodic box using N Fourier modes in each direction. For a given quantity, the physical Q and the spectral $\hat{Q}$ representations are related using the direct and the inverse discrete Fourier transforms:

$$\hat{Q}(\mathbf{k}) = \frac{1}{N^3} \sum_{\mathbf{x}} Q(\mathbf{x}) e^{-ik_j x_j} \,, \tag{4}$$

$$Q(\mathbf{x}) = \sum_{\mathbf{k}} \hat{Q}(\mathbf{k}) e^{ik_j x_j} \,. \tag{5}$$

The spectral representations of the equations (1)-(2), are easily derived and read:

$$\frac{\partial \hat{u}_i(\mathbf{k})}{\partial t} = -ik_j \sum_{\mathbf{p}} \hat{u}_j(\mathbf{k}-\mathbf{p})\hat{u}_i(\mathbf{p}) + ik_j \sum_{\mathbf{p}} \hat{b}_j(\mathbf{k}-\mathbf{p})\hat{b}_i(\mathbf{p}) + ik_j B_j^0 \hat{b}_i(\mathbf{k}) - \nu k^2 \hat{u}_i(\mathbf{k}) + \hat{f}_i(\mathbf{k}) - ik_i \hat{p}(\mathbf{k}) \,, \tag{6}$$

$$\frac{\partial \hat{b}_i(\mathbf{k})}{\partial t} = -ik_j \sum_{\mathbf{p}} \hat{u}_j(\mathbf{k}-\mathbf{p})\hat{b}_i(\mathbf{p}) + ik_j \sum_{\mathbf{p}} \hat{b}_j(\mathbf{k}-\mathbf{p})\hat{u}_i(\mathbf{p}) + ik_j B_j^0 \hat{u}_i(\mathbf{k}) - \eta k^2 \hat{b}_i(\mathbf{k}) \,. \tag{7}$$

The evolution of the kinetic energy ($E^u(\mathbf{k}) = \frac{1}{2}|\hat{\mathbf{u}}(\mathbf{k})|^2$) and the magnetic energy ($E^b(\mathbf{k}) = \frac{1}{2}|\hat{\mathbf{b}}(\mathbf{k})|^2$) carried on by the modes with wave vector $\mathbf{k}$ are easily derived from these equations and their complex conjugates:

$$\frac{\partial}{\partial t} E^u(\mathbf{k}) = N_u^u(\mathbf{k}) + N_b^u(\mathbf{k}) + L_{ub}(\mathbf{k}) - 2\nu k^2 E^u(\mathbf{k}) + I_f(\mathbf{k}) \,, \tag{8}$$

$$\frac{\partial}{\partial t} E^b(\mathbf{k}) = N_b^b(\mathbf{k}) + N_u^b(\mathbf{k}) - L_{ub}(\mathbf{k}) - 2\eta k^2 E^b(\mathbf{k}) \,, \tag{9}$$

where

$$I^f(\mathbf{k}) = \frac{1}{2} \Re \left\{ \hat{f}_i(\mathbf{k}) \hat{u}_i^*(\mathbf{k}) + \hat{f}_i^*(\mathbf{k}) \hat{u}_i(\mathbf{k}) \right\} \,, \tag{10}$$

$$L_{ub}(\mathbf{k}) = \frac{1}{2} k_j B_j^0 \, \Im \left\{ \hat{u}_i(\mathbf{k}) \hat{b}_i^*(\mathbf{k}) - \hat{u}_i^*(\mathbf{k}) \hat{b}_i(\mathbf{k}) \right\} \,, \tag{11}$$

and where $\Re$ and $\Im$ represent respectively the real and imaginary part of a complex number and * denotes the complex conjugation. The quantities $N_Y^X(\mathbf{k})$ are defined as

follows:

$$N_u^u(\mathbf{k}) = \frac{1}{2}\sum_{\mathbf{p}} \Re\{-[ik_j\hat{u}_j(\mathbf{k}-\mathbf{p})][\hat{u}_i(\mathbf{p})\hat{u}_i^*(\mathbf{k})] + [ik_j\hat{u}_j^*(\mathbf{k}-\mathbf{p})][\hat{u}_i^*(\mathbf{p})\hat{u}_i(\mathbf{k})]\}\,, \tag{12}$$

$$N_b^u(\mathbf{k}) = \frac{1}{2}\sum_{\mathbf{p}} \Re\{+[ik_j\hat{b}_j(\mathbf{k}-\mathbf{p})][\hat{b}_i(\mathbf{p})\hat{u}_i^*(\mathbf{k})] - [ik_j\hat{b}_j^*(\mathbf{k}-\mathbf{p})][\hat{b}_i^*(\mathbf{p})\hat{u}_i(\mathbf{k})]\}\,, \tag{13}$$

$$N_b^b(\mathbf{k}) = \frac{1}{2}\sum_{\mathbf{p}} \Re\{-[ik_j\hat{u}_j(\mathbf{k}-\mathbf{p})][\hat{b}_i(\mathbf{p})\hat{b}_i^*(\mathbf{k})] + [ik_j\hat{u}_j^*(\mathbf{k}-\mathbf{p})][\hat{b}_i^*(\mathbf{p})\hat{b}_i(\mathbf{k})]\}\,, \tag{14}$$

$$N_u^b(\mathbf{k}) = \frac{1}{2}\sum_{\mathbf{p}} \Re\{+[ik_j\hat{b}_j(\mathbf{k}-\mathbf{p})][\hat{u}_i(\mathbf{p})\hat{b}_i^*(\mathbf{k})] - [ik_j\hat{b}_j^*(\mathbf{k}-\mathbf{p})][\hat{u}_i^*(\mathbf{p})\hat{b}_i(\mathbf{k})]\}\,, \tag{15}$$

and represents the energy transfer to mode $\mathbf{k}$ of field X to all the modes $\mathbf{p}$ of field Y. Furthermore we can decompose $N_Y^X(\mathbf{k})$ into a series of transfer functions $T_{Y(\mathbf{p})}^{X(\mathbf{k})}$, representing the energy transfer to mode $\mathbf{k}$ of field X from mode $\mathbf{p}$ of field Y, such that:

$$N_Y^X(\mathbf{k}) = \sum_{\mathbf{p}} T_{Y(\mathbf{p})}^{X(\mathbf{k})} \tag{16}$$

The energy equations contain non-linear N_Y^X and linear L_{ub} transfer terms as well as dissipative terms proportional to ν and η and source (energy injection) terms I^f. A statistically stationary state is reached when the turbulence is fully developed. For this state, the energy injected by the force $\hat{f}_i$ is equal to the energy losses due to kinetic and magnetic dissipative effects. Moreover, the energy content of the spectral modes is also stationary in this state. However, the fluctuations in the energy balance for a single mode [Eqs. (8) or (9)] are very large, hence for meaningful statistical result we need to average over a Fourier sub-domain containing enough similar modes. If the number of modes is too low, a time-averaging can also be used to improve the convergence of the results. The choice of the partition of the Fourier space into disjoint subdomains is motivated by the physical properties of the flow. Each sub-domain is indeed expected to represent a set of modes with similar properties. However, at this stage, it is not necessary to give an explicit definition for this partitioning and it will be only assumed to be characterized by two integer indices $\{m, \alpha\}$. The choice of a sharp decomposition of the spectral space (disjoint subdomains) compared to a smooth decomposition (overlapping subdomains) has been validated by the studies [9] and [10]. The equation for the energy stored in each of the sub-domain is thus trivially derived from Eqs. (8-9):

$$\frac{\partial}{\partial t}E^{u\{m,\alpha\}} = N_u^{u\{m,\alpha\}} + N_b^{u\{m,\alpha\}} + L_{ub}^{\{m,\alpha\}} - D^{u\{m,\alpha\}} + I^{f\{m,\alpha\}}\,, \tag{17}$$

$$\frac{\partial}{\partial t}E^{b\{m,\alpha\}} = N_b^{b\{m,\alpha\}} + N_u^{b\{m,\alpha\}} - L_{ub}^{\{m,\alpha\}} - D^{b\{m,\alpha\}}\,. \tag{18}$$

The energy evolution equations first contain contribution from the nonlinearities in the MHD equations. These terms,

$$N_Y^{X\{m,\alpha\}} \equiv \sum_{\{n,\beta\}} T_{Y\{n,\beta\}}^{X\{m,\alpha\}}\,, \tag{19}$$

correspond to the sum of the nonlinear energy transfers $T_{Y\{n,\beta\}}^{X\{m,\alpha\}}$ to the field X in the ring $\{m, \alpha\}$ from the field Y in the ring $\{n, \beta\}$. Each of these nonlinear transfers is itself the

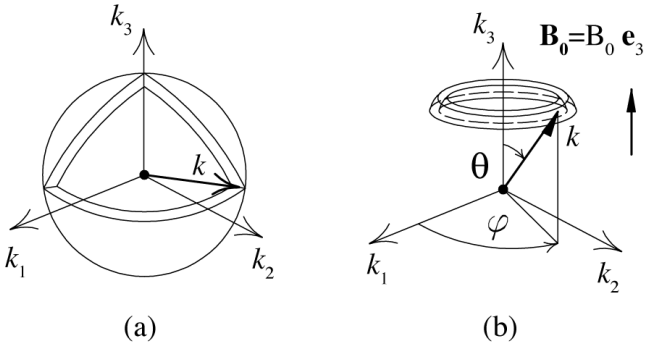

Figure 1: a) Shell decomposition; b) Ring decomposition.

sum of mode-to-mode transfers:

$$T_{Y\{n,\beta\}}^{X\{m,\alpha\}} = \sum_{\mathbf{k}\in\{m,\alpha\}} \sum_{\mathbf{p}\in\{n,\beta\}} T_{Y(\mathbf{p})}^{X(\mathbf{k})} \,, \tag{20}$$

The major advantage of these definitions is that they naturally satisfies the following expected antisymmetry property [7, 8]:

$$T_{Y\{n,\beta\}}^{X\{m,\alpha\}} = -T_{X\{m,\alpha\}}^{Y\{n,\beta\}} \,. \tag{21}$$

The other quantities Q in the Eqs. (17-18) are defined as the selection over the modes $\mathbf{k}$:

$$Q^{X\{m,\alpha\}} = \sum_{\mathbf{k}\in\{m,\alpha\}} Q^X(\mathbf{k}) \,. \tag{22}$$

In the following section, the Fourier space partitioning is based on a ring decomposition. The first index m in the partition $\{m,\alpha\}$ corresponds to the spherical shell decomposition, commonly used in the investigation of isotropic turbulence. It is based on the division of the spectral space along the wave-vector norm k. A shell s_m contains all the wave-vectors $\mathbf{k}$ with the property $k_m \leq |\mathbf{k}| < k_{m+1}$ (Figure 1a). The set of shell boundaries $\{k_m\}$ may of course depend on the problem. The second index α corresponds to the angular dependency. For simplicity, the mean magnetic field is assumed to be aligned with $\mathbf{1}_z$. The wave-vector $\mathbf{k}$ forms an angle θ with respect to the B^0, $\theta \in [0,\pi]$. The spectral domain is split into angular sections a_α so that each section contains the wave-vectors that have the angle θ bounded by $\theta_{\alpha-1} \leq \theta < \theta_\alpha$. The intersection between the spherical shells and the angular sections defines the ring structures $r_{m\alpha} = s_m \cap a_\alpha$ (Figure 1.b). The rings near $\theta = \pi/2$ will be referred to as *equatorial rings*, and the rings near $\theta = 0$ as *polar rings*. The shell-to-shell energy can be computed by summing the ring-to-ring energy transfers over the angular sections:

$$T_{Y\{n\}}^{X\{m\}} = \sum_{\alpha}\sum_{\beta} T_{Y\{n,\beta\}}^{X\{m,\alpha\}} \,. \tag{23}$$

From the ring-to-ring transfers we can also determine the radial energy flux (coming out of a wave-number sphere)

$$\Pi_{Y_<}^{X_>}(k_l) = \sum_{n<l}\sum_{\beta}\sum_{m\geq l}\sum_{\alpha} T_{Y\{n,\beta\}}^{X\{m,\alpha\}} \,, \tag{24}$$

and the angular energy flux (coming into a cone of angle θ_γ)

$$\Pi_{Y<}^{X>}(\theta_\gamma) = \sum_n \sum_{\beta<\gamma} \sum_m \sum_{\alpha\geq\gamma} T_{Y\{n,\beta\}}^{X\{m,\alpha\}} \,. \tag{25}$$

The expression for the energy transfers between two rings is somewhat arbitrary, however, the fluxes (24) and (25) are unambiguous because they represent the total energy leaving due to a given non-linear term.

3 Numerical results

The MHD equations are solved by a pseudo-spectral code [11] in a box with periodic boundaries conditions. By taking the length of the box $\mathcal{L} = 2\pi$, we chose the smallest wave-number of our simulation as $k^{\min} = 1$. Selecting a resolution of $N = 512$ modes in each direction limits the largest wave-number to $k^{\max} = 256$. Performing a direct numerical simulation (DNS) of a turbulent flow requires that the largest and the smallest physical lengths are contained in the scale range solved by our simulation. In practice, we need to check that the largest (integral length L_i^X) and smallest (Kolmogorov length l_K^X) scales for the flow and for the magnetic field are well captured by the grid. For X standing in for u or b, we have the definitions:

$$L_i^X = \frac{4\pi}{3} \frac{\int k^{-1} E^X(k) dk}{\int E^X(k) dk} \tag{26}$$

$$l_K^X = (\xi^3/\varepsilon)^{1/4} \tag{27}$$

where $\xi = \nu$ for the fluid Kolmogorov length and $\xi = \eta$ for the magnetic Kolmogorov length. ε represents the total dissipation of the system (kinetic+magnetic). For a proper DNS simulation, taking $L_i = MAX\{L_i^u, L_i^b\}$ and $l_K = MIN\{l_K^u, l_K^b\}$ we have to check the conditions $k^{\min} L_i < 1$ and $k^{\max} l_K > 1$ are true.

The solver computes the nonlinear terms in real space, passing from the complex to the real space and back via a Fast Fourier Transform algorithm (FFT). Aliasing errors are removed using a phase shift method (an approximative dealiasing method). The time step is computed automatically by a CFL criteria and the time advancement is based on a third order Runge-Kutta scheme.

Starting from random initial conditions with a prescribed energy spectrum and random phases, the forced MHD equations are evolved. The force used in the present work is local in Fourier space. This choice ensures that each of the $N_f = 104$ forced modes with $\mathbf{k}$ ($k_{\text{inf}} = 2.4 \leqslant |\mathbf{k}| < k_{\text{sup}} = 3.1$) contained in the forcing shell $s_f = [k_{\text{inf}}, k_{\text{sup}}]$ is submitted to a forcing mechanism that injects energy at the rate $\varepsilon_e(\mathbf{k}) = \epsilon_e/N_f$ and helicity at the rate $\varepsilon_h(\mathbf{k}) = \epsilon_h/N_f$. The total energy and helicity desired to be injected by the force are respectively ϵ_e and ϵ_h and represent the forcing control parameters along with the forcing shell s_f. The force $\hat{\mathbf{f}}$ has the following form:

$$\hat{\mathbf{f}}(\mathbf{k}) = \alpha(\mathbf{k})\hat{\mathbf{u}}(\mathbf{k}) + \beta(\mathbf{k})\hat{\omega}(\mathbf{k}) \tag{28}$$

if $|\mathbf{k}| \in s_f$ and zero otherwise. The vector $\hat{\omega}(\mathbf{k})$ represents the Fourier modes of the vorticity ($\omega = \nabla \times \mathbf{u}$). Defining the helicity as $H(\mathbf{k}) = \Re\{\hat{\mathbf{u}}(\mathbf{k}) \cdot \hat{\omega}^*(\mathbf{k})\}$, we obtain the

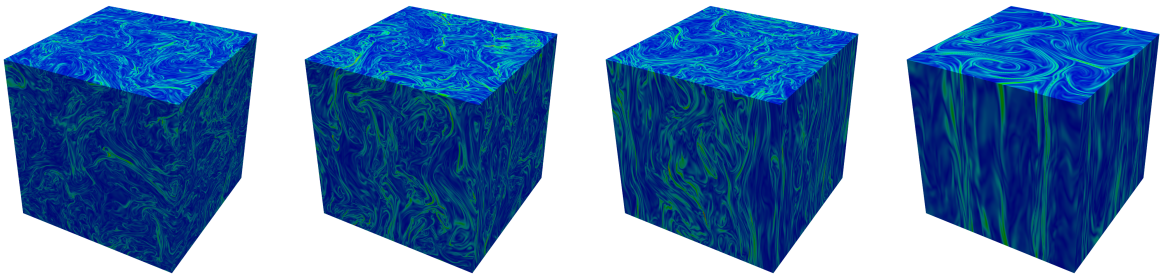

Figure 2: Vorticity density in real space. Lighter colors denotes higher $|\omega|$values. Left to right we see the isotropic case ($|B^0| = 0$), weak anisotropic case ($|B^0| = \delta b^{\text{iso}}$), strong anisotropic ($|B^0| = \sqrt{10}\,\delta b^{\text{iso}}$) case and $|B^0| = \sqrt{100}\,\delta b^{\text{iso}}$ case.

real parameters $\alpha(\mathbf{k})$ and $\beta(\mathbf{k})$ as:

$$\begin{cases} \alpha(\mathbf{k}) = \dfrac{1}{2N_f} \dfrac{4k^2 E^u(\mathbf{k})\varepsilon_e(\mathbf{k}) - H(\mathbf{k})\varepsilon_h(\mathbf{k})}{4k^2 E^u(\mathbf{k})^2 - H(\mathbf{k})^2} \\ \beta(\mathbf{k}) = \dfrac{1}{N_f} \dfrac{H(\mathbf{k})\varepsilon_e(\mathbf{k}) - E^u(\mathbf{k})\varepsilon_h(\mathbf{k})}{4k^2 E^u(\mathbf{k})^2 - H(\mathbf{k})^2} \end{cases} \tag{29}$$

Since the energy injection rate ϵ_e due to the forcing is split equally between the 104 modes contained in the s_f wave-number shell, the forcing is isotropic and acts only in the large scale. In the present study, no helicity is injected by the forcing process.

For the statistical steady state, when the total dissipation ε equals the energy injection rate ϵ_e, the Taylor micro-scale Reynolds number reaches $R_\lambda \approx 210$. The product between the Kolmogorov length and the largest wave-number is about $k^{\max} l_K \approx 1.23$ and between the integral length scale and the smallest wave-number is $k^{\min} L_i \approx 0.78$, ensuring that the smallest physical scale and the largest physical scales are well resolved by our simulation.

A first computation has been performed without external magnetic field ($B^0 = 0$), which will be referred to as the isotropic run. Once the statistically stationary state is reached, the fluctuations of the magnetic field in isotropic turbulence are measured using the following quantity:

$$\delta b^{\text{iso}} = \left(\frac{1}{\mathcal{L}^3} \int d^3\mathbf{x}\; \mathbf{b}(\mathbf{x},t) \cdot \mathbf{b}(\mathbf{x},t) \right)^{1/2} . \tag{30}$$

Two values of B^0 have been considered for in depth analysis, corresponding respectively to $|B^0| = \delta b^{\text{iso}}$ and $|B^0| = \sqrt{10}\,\delta b^{\text{iso}}$. These two computations will be referred to as the weakly anisotropic run and the strongly anisotropic run respectively. The ambient magnetic field will have a tendency to align the fluid eddies along its direction. This effect can be observed by looking at vorticity (ω) in real space (see Figure 2). The $|B^0| = \sqrt{100}\,\delta b^{\text{iso}}$ case, although not studied, is listed for comparison. It represents an extreme case of anisotropy, where the turbulence is quasi 2D. Since the one-dimensional integral length scale is as large as the computational box, the large scale eddies in the direction of the external magnetic field are affected by non-physical self-interaction. Such case although useful as a model can not be considered as a reasonable DNS.

The ambient magnetic field is turned on at the time t_0 (see Figure 3). The force is identical for the three runs. For that reason the total dissipation rate is equal for the three cases. Is is known from decaying simulations that the palenstrophy is amplified in the presence of a external magnetic field which in turn will diminish the dissipation rate of the total energy. Since the dissipation level reaches equilibrium with the energy

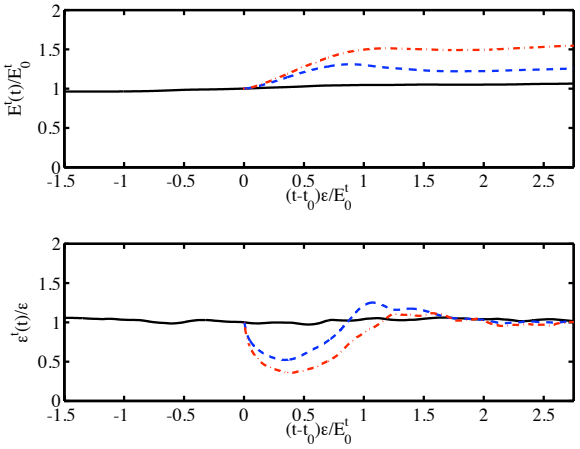

Figure 3: Total energy ($E^t = E^u + E^b$) and total dissipation ($\epsilon^t = \epsilon^u + \epsilon^b$) evolution in time. The time at which the external magnetic was switched on is denoted by t_0 and the quantities at that time are indexed by 0. The isotropic case is represented by the plain (black) line, the weak anisotropic case is denoted by the dashed (blue) line and the strong anisotropic case is denoted by the dot-dashed (red) line.

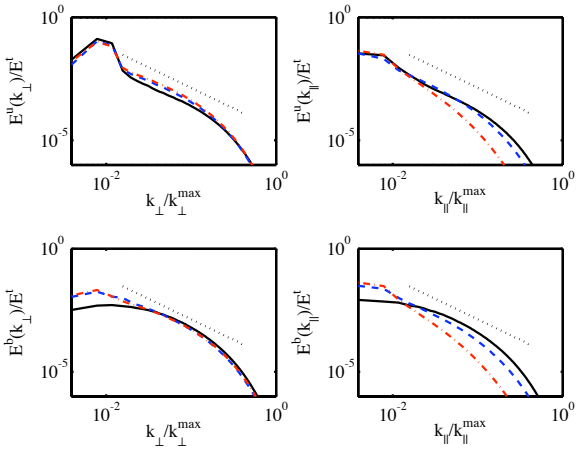

Figure 4: Kinetic (E^u) and magnetic (E^b) spectra. The isotropic case is represented by the plain (black) line, the weak anisotropic case is denoted by the dashed (blue) line and the strong anisotropic case is denoted by the dot-dashed (red) line. The dotted line represents the $k^{-5/3}$ slope.

injected by the external force, we notice a rise in energy levels in the presence of B^0. This fact shows that the dynamical processes involved in the dissipation suppression for the decaying case are present for the forced case as well.

We first split the spectral space ito cylinders of unity width and we look at the energy as a function of the perpendicular ($k_\perp = (k_x^2 + k_y^2)^{1/2}$) and parallel ($k_\parallel = k_z$) wave-numbers. The energy per mode $E^X[k_x, k_y, k_z]$ of the variable $X = u$ or $X = b$ can be integrated using cylindrical coordinates to obtain the energy per perpendicular and parallel modes:

$$E^X(k_\perp, k_\parallel) = \int k_\perp E^X(k_x[k_\perp, \varphi], k_y[k_\perp, \varphi], k_z[k_\parallel] d\varphi \,, \tag{31}$$

$$E^X(k_\perp) = \int E^X(k_\perp, k_\parallel) dk_\parallel \,, \tag{32}$$

$$E^X(k_\parallel) = \int E^X(k_\perp, k_\parallel) dk_\perp \,. \tag{33}$$

The spectra are shown in Figure 4 in which the influence of the ambient magnetic field can be seen. the iso-countours of the quantity $E(k_\perp, k_\parallel)$ give a better idea how the energy distribution varies with the angle between the wave-vector and the direction of the constant magnetic field (Figure 5). Clearly, the energy levels do not exhibit a strong angular dependence in the weakly anisotropic run but the strong anisotropic case shows that a traditional shell decomposition of the Fourier space is probably not adapted for this case.

The analysis of the energy transfers is based on a partition of the Fourier space using 23 spherical shells and 15 angular sections. The shells are defined by $s_n = [k_n, k_{n+1}]$, in which k_n is given by the law $k_n = 2^{(n+8)/4}$. The first three shells are however defined

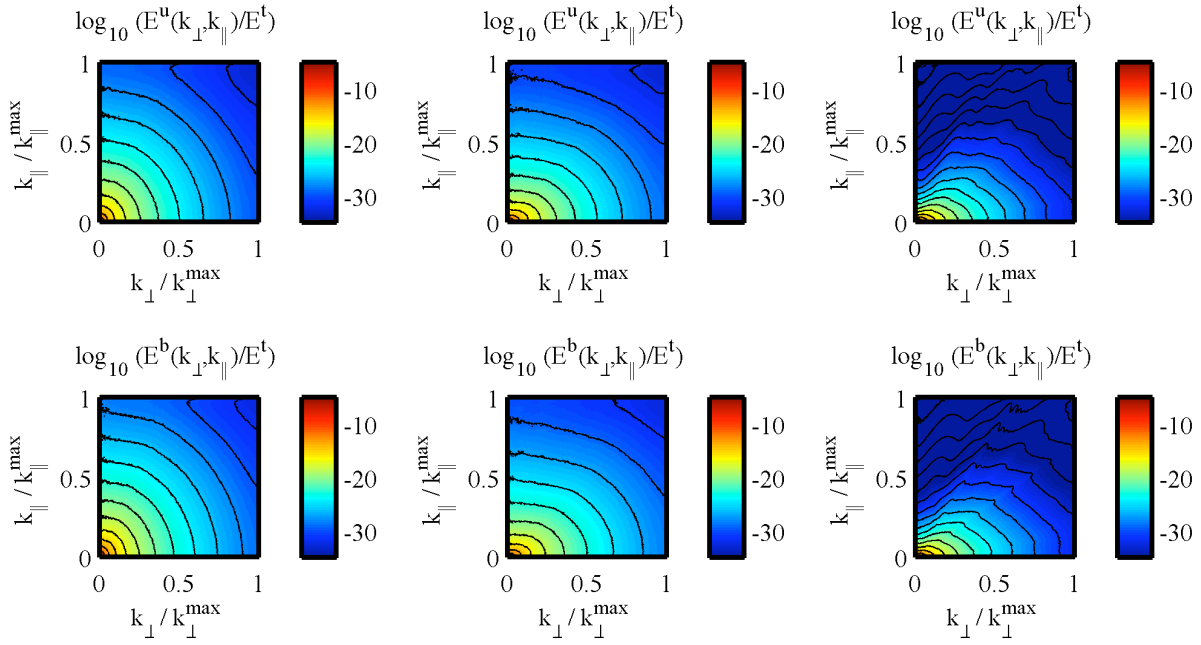

Figure 5: Representation of the logarithms ($\log_{10}$) of the kinetic (top) and of the magnetic (bottom) energies. Left to right indicate the isotropic, weakly anisotropic and strongly anisotropic runs. The values are normalized to the total energy for each case. Black lines show energy iso-value contours

differently, $s_1 = [0, 2]$, $s_2 = [2, 4]$, $s_3 = [4, 8]$, in order to ensure that these shells contain enough modes. The angular sections are taken as constant, with an angular separation of 12°. The eighth angular section is centered on the equatorial plane. The forcing is isotropic and acts only in the shell s_2. The force is identical for the three runs. In the figures presented below, the three-dimensional Fourier space is projected on a plane in which the shells s_n are represented by annuli with a width proportional to $k_{n+1} - k_n$. The plane is further split into the angular sections a_α. The intersections of the annuli and the angular sections represent the projections of the rings into a plane and the intensity of the variables in these rings are color coded. Only half of the plane is represented since each rings has two symmetric intersections with it. As a first example of this representation, the kinetic and magnetic energies are shown in Figure 6.

Dissipation level are represented in Figure 7. For all three cases, the total magnetic dissipation is about twice the total kinetic dissipation. Since the total dissipation has to be equal to the energy injection rate, the respective levels of kinetic and magnetic dissipation are thus almost the same in the three runs. In the isotropic run, no angular variation is observed up to slight fluctuations. On the contrary, in the anisotropic runs, the levels of dissipation are clearly angle dependent. The dissipation in the direction of B_0 tends to be suppressed, and this effect increases with the imposed magnetic field. Since global kinetic and magnetic dissipation are about the same as in the isotropic case, the decrease of dissipation in the direction parallel to the constant magnetic field has to be compensated by an increase of dissipation in the perpendicular direction. This behavior is stronger for larger degrees of anisotropy.

By summing over the angular sections, we find the shell-to-shell energy transfers, represented in Figure 8. If $T_{Y\{n\}}^{X\{m\}}$ is positive, the shell variable m is receiving energy from the shell variable n. The symmetry relation (21) automatically implies that, in this case,

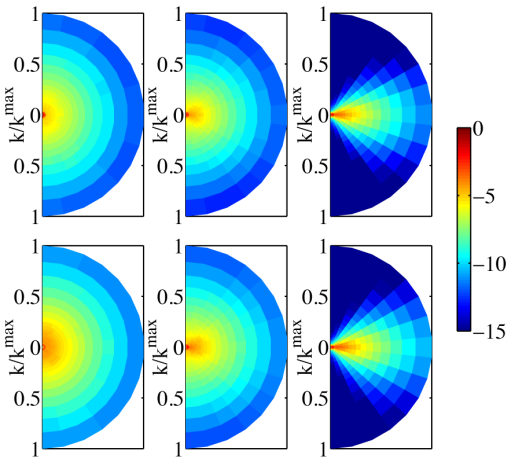

Figure 6: Ring representation of the logarithms ($\log_{10}$) of the kinetic (top) and of the magnetic (bottom) energies. Left to right columns indicate the isotropic, weakly anisotropic and strongly anisotropic runs. The values are normalized to the total energy. The plots take into account the width of the shell for which the boundaries have been normalized to the largest wavenumber $k^{\max}$.

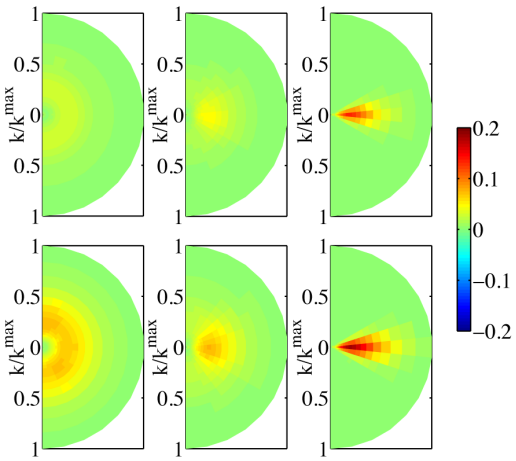

Figure 7: Ring representation of the kinetic (top) and of the magnetic (bottom) dissipation. Left to right columns indicate the isotropic, weakly anisotropic and strongly anisotropic runs. The values displayed are normalized to the total dissipation ε. The plots take into account the width of the shell for which the boundaries have been normalized to the largest wavenumber $k^{\max}$.

the shell variable n is loosing energy at the expense of shell variable m. When $T^{X\{m\}}_{Y\{n\}}$ is positive for $m > n$, the situation is referred to as a "forward" energy transfer. Otherwise, it is referred to as a "backward" energy transfer. When the largest (positive as well as negative) value of $T^{X\{m\}}_{Y\{n\}}$ are observed for n close to m, the energy transfer is referred to as "local". It is important to realize that the locality of the energy transfer has to be interpreted as energy exchanges between structures that have similar length scales and not necessarily between positions that are close to each other in the physical space.

As expected from the phenomenology of turbulence, the energy transfers $T^{u\{m\}}_{u\{n\}}$ and $T^{b\{m\}}_{b\{n\}}$ are essentially local and forward. Locality can be observed since all the significant transfers are along the diagonal where n is close m. Only direct transfers are observed which is confirmed by positive value below the diagonal and negative value above. Also, scale independent energy transfers can be observed since all the horizontal lines are very much similar when properly shifted by m boxes, i.e. $T^{X\{m\}}_{Y\{n\}}$ is essentially a function of $m - n$ and not of n and m separately. Such properties confirm previous results. In forced turbulence, non-local interactions between the velocity and the magnetic fields are observed. These non-local interactions are clearly related to the forcing and only affect the forced velocity shell which transfers energy to the magnetic field at almost all scales.

It is interesting to note that the shell-to-shell transfers are completely unsuited for anisotropic study. Comparing the shell-to-shell transfers for the isotropic and the anisotropic cases (Figure 8), we obtain similar information. More important, we cannot properly distinguish between the isotropic and the anisotropic cases. A backward cross field energy transfer is observed for the weak anisotropic case but it vanishes for the strong anisotropic case. For this reason, we make use of the ring-to-ring transfers.

The complete description of ring-to-ring energy transfers $T^{X\{m,\alpha\}}_{Y\{m,\beta\}}$ would require a four-dimensional representation or a large number of two-dimensional figures. Instead of a long

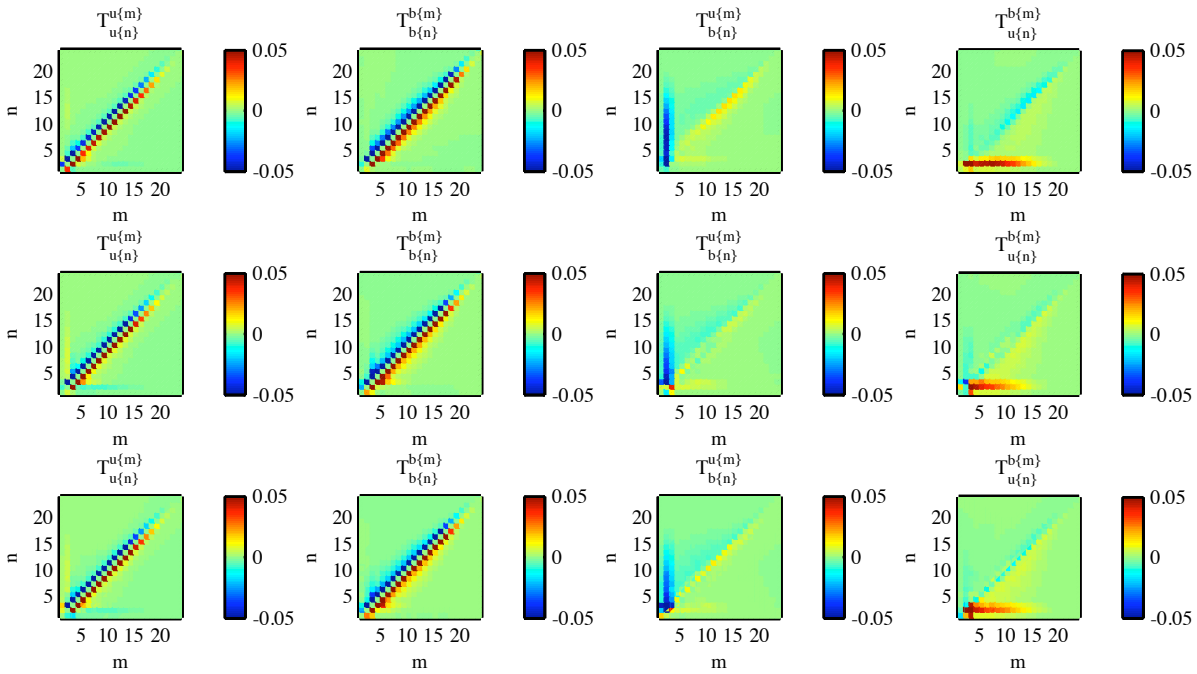

Figure 8: Shell-to-shell energy transfers for the isotropic case (top), the weak anisotropic case (middle) and strong anisotropic case (bottom). The energy is transfered from shell n to shell m.

collection of figures, we first present the total energy transferred to a ring from all the other rings ($N_Y^{X\{m,\alpha\}}$) in Figure 9. The angular dependency of the transfer functions is evident. It is interesting to observe that the cross-field transfer (between the velocity and the magnetic fields) changes sign depending on the direction to B_0 for the anisotropic cases.

A more detailed picture of the energy exchange can be obtained from the analysis of the ring-to-ring transfer functions (not shown). Using the ring decomposition we can quantify the angular transfers. For the anisotropic cases, the energy flows towards the equator (direction perpendicular to the mean magnetic field) and the energy transfer are strongest near the equator.

4 Conclusions

DNS of forced MHD turbulence are analyzed for isotropic and anisotropic conditions. The source of anisotropy has been assumed to be an external ambient magnetic field $\mathbf{B}^0$. Three runs have been compared. One run corresponds to the isotropic system ($\mathbf{B}^0 = 0$) and the two other cases have nonzero $\mathbf{B}^0$ and have been referred to as the weakly and strongly anisotropic runs.

Using a shell decomposition of the velocity and magnetic fields, we observe that the kinetic and magnetic energy cascades are essentially forward and local, although a non-local transfer of energy between the forced velocity shell and the small scale magnetic field is observed. These non-local interactions are clearly related to the forcing and only affect the forced velocity shell which transfers energy to the magnetic field at almost all scales. Considering similar independent results [4] obtained using another type of forcing, it seems that this phenomenon is independent of the nature of the forcing. Since similar results are found for the anisotropic cases we reach the conclusion that a shell spectral

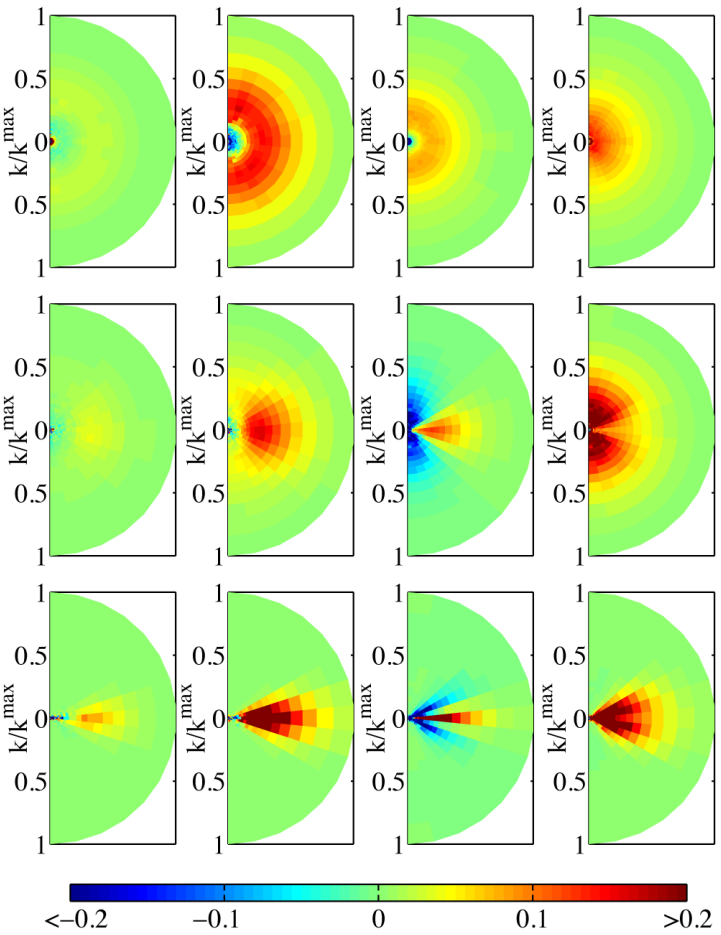

Figure 9: The net energy transfer to each ring. Left to right columns indicate: $N_u^{u\{m,\alpha\}}$, $N_b^{b\{m,\alpha\}}$, $N_b^{u\{m,\alpha\}}$ and $N_u^{b\{m,\alpha\}}$. Top to bottom represent the isotropic, weakly anisotropic and strongly anisotropic runs. The values displayed are normalized to the total dissipation ε. The plots take into account the width of the each shell for which the boundaries have been normalized to the largest wave-number $k^{\max}$.

decomposition is not well suited for anisotropic simulations.

We use a ring decomposition of the spectral space and look at the energy transfer in anisotropic MHD turbulence. The energy, energy dissipation, and energy transfers in the presence of a constant magnetic field have been shown to depend on the angular section. The anisotropy becomes more pronounced when the strength of the mean magnetic field is increased.

We have analysed the energy transfers among various rings in the spectral space. We observe that the dominant energy transfer is in the direction perpendicular to the mean magnetic field, and the energy transfers parallel to the mean magnetic field is suppressed. These results are in agreement with the results reported in the past. Our studies show that the energy transfers among the rings are also local and forward, i.e., the dominant energy transfer is to the nearest rings, and the direction is from smaller wave-number rings to larger wave-number rings.

Acknowledgements

The authors would like to acknowledge Bernard Knaepen, Paolo Burattini and Maxim Kinet for useful discussions. MKV thanks the Physique Statistique et Plasmas group at the University Libre de Bruxelles for the kind hospitality and financial support during his long leave when this work was undertaken. DC is supported by the Fonds National pour la Recherche Scientifique F.N.R.S.-Belgium.

References

[1] M. Lesieur, *Turbulence in Fluids*, (Kluwer Academic Publisher, Dordrecht, 1997).

[2] J.A. Domaradzki and R.S. Rogallo, Phys. Fluids A **2**, 413 (1990).

[3] A. Alexakis, P.D. Mininni, and A. Pouquet, Phys. Rev. E **72**, 046301 (2005).

[4] P.D. Mininni, A. Alexakis, and A. Pouquet, Phys. Rev. E **72**, 046302 (2005).

[5] O. Debliquy, M.K. Verma, and D. Carati, Phys. Plasmas **12**, 042309 (2005).

[6] A. Alexakis, B. Bigot, H. Politano, and S. Galtier, Phys. Rev. E **76**, 056313 (2007).

[7] G. Dar, M.K. Verma, and V. Eswaran, Physica D **3**, 207 (2001).

[8] M.K. Verma, Phys. Report **401**, 229 (2004).

[9] J.A. Domaradzki and D. Carati, Physics. Fluids. **19**, 085111 (2007).

[10] J.A. Domaradzki and D. Carati, Physics. Fluids. **19**, 085112 (2007).

[11] D. Carati & TURBO team, *Solver for TURbulent flows with periodic BOundary conditions*, http://www.ulb.ac.be/sciences/spp (2008).

[12] D. Carati, O. Debliquy, B. Knaepen, B. Teaca, and M.K. Verma, J. of Turbulence **7 N51**, 1 (2006).

[13] P. Burattini, M. Kinet, D. Carati, and B. Knaepen, Phys. Fluids **20**, 065110 (2008).

[14] P. Burattini, M. Kinet, D. Carati, and B. Knaepen, Physica D **237**, 2062 (2008).

[15] M. Kinet, P. Burattini, D. Carati, and B. Knaepen, Phys. Fluids **20**, 075105 (2008).

[16] R. Kraichnan, J. Fluid Mech. **47**, 525 (1971).

[17] A. Potherat and T. Alboussiere, Physics of Fluids **15**,3170 (2003).

[18] W. H. Matthaeus, S. Ghosh, S. Oughton, and D. A. Roberts, J. Geophys. Res. **101**, 7619 (1996).

[19] O. Schilling and Y. Zhou, J. Plasma Phys. **68**, 389 (2002).

[20] L. Biferale, E Calzavarini, A.S. Lanotte, F. Toschi, and R. Tripiccione, Physica A **338**, 194 (2004).

[21] J. Cho and E.T. Vishniac, ApJ **539**, 273 (2000)

[22] J. Maron and P. Goldreich, ApJ **554**, 1175 (2001)